

Wavefront construction using waverays

*Hector Urdaneta*¹

ABSTRACT

A method for computing first arrival traveltimes and amplitudes in a general two-dimensional (2-D) velocity model is presented. The method is the result of merging two recently published ray tracing methods. The product is a very robust algorithm that is able to produce broadband wave phenomena, such as dispersion and wavelength dependent scattering. Its ability to produce broadband wave phenomena, is achieved by performing a wavelength-dependent smoothing of the velocity model across wavefronts. In the limit of high frequency, the method reduces to geometrical ray theory. The method is able to illuminate areas of large geometrical spreading where conventional ray tracing methods may give no arrivals. The method is tested on synthetic complex velocity models.

INTRODUCTION

Traditionally traveltime and amplitude calculations have been performed by ray tracing. Different ray tracing algorithms exist that are well known and well documented. They include Julian and Gubbins' (1977) ray bending, Dines and Lytle's (1979) shooting rays and Červený's (1987) paraxial extrapolation. More recently, several new methods have appeared and are enjoying an increasing popularity. They include Vidale (1990), Podvin and Lecomte (1991), van Trier and Symes (1991) finite differences and Moser's (1991) shortest path rays. This paper presents a review of two new ray tracing methods and explores some of the possibilities produced by their fusion. The first method is Lomax's (1994) waveray method for approximating broadband wave propagation through complex velocity structures. The second method was developed at the NORSAR institute in Norway by Vinje, Iversen and Gjøystdal (1993). As will be shown later, both methods have their own advantages and drawbacks, but when they are fused, they interfere positively. The combined product produces a very robust method, which approximates broadband wave phenomena in complex velocity models. The first two parts of this paper describe the basic characteristics of each method and their implementations. The paper also reviews some of the work done in the last two references listed above. In the last part, I discuss the combined method. Implementation issues and synthetic examples are shown.

¹email: not available

LOMAX'S WAVERAYS

Two basic ideas characterize Lomax's method: (1) it does a wavelength-dependent velocity smoothing and (2) it uses Huygen's principle to track the motion of narrow-band wavefronts at a number of center frequencies. Narrow-band wavefronts are defined as surfaces (lines in 2-D) of constant phase or traveltime in a narrow-band "wavefield". As these narrow-band wavefronts propagate with time they define a wavepath, which is frequency dependent. The wavelength-dependent smoothing of the velocity is done by averaging with a Gaussian weighting curve. The smoothing is done along the wavefronts. The final result; i.e, the broadband wavefield, is constructed by summing the results of independent narrow-band wavefields at many center frequencies. Three important advantages of using Lomax's waveray over conventional ray tracing methods are:

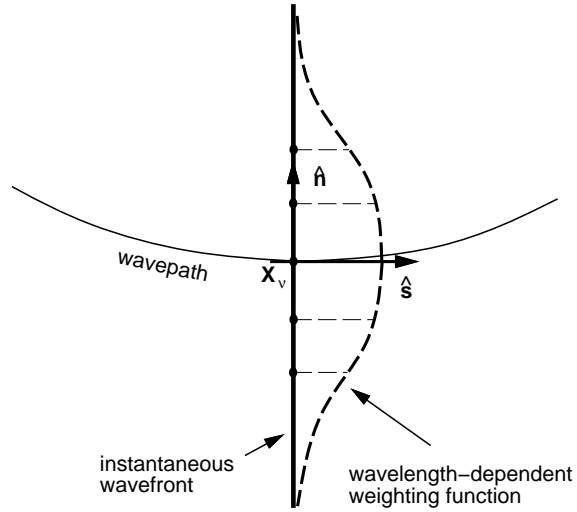
- It increases the stability of wavepaths compared to the paths produced by high frequency methods, due to the wavelength-dependent smoothing.
- It provides waverays with a sensitivity that produces frequency dependent scattering as a function of the ratio of wavelength to the characteristic size of the scattering region. Figure 3 illustrates this point.
- It is capable of handling large to small inhomogeneity sizes, since in the former case it is similar to ray theory and in the latter it responds to a smooth, averaged velocity structure.

In Lomax (1994), the author approximates the narrow-band wavefronts at any time by a plane wavefront (see Figure 1). This approximation requires that the radius of curvature of the wavefront be large relative to a wavelength. A better approximation to the wavefronts could probably be obtained using a parabolic approximation. For the sake of computational time, plane wavefronts are used. Before considering the details of the waveray technique, two points need to be emphasized. First, Lomax (1994) points out, "it is the wavelength dependent smoothing that makes the waveray method a broadband wave propagation technique, and distinguishes it from the high frequency ray methods." Second, there are no equations that give the waveray method a theoretical basis. Its support comes from the fact that it reproduces high-frequency ray propagation and produces a good approximation of broadband wave phenomena.

Waveray implementation

In the waveray method, the wavelength-dependent averaging of the velocity is done dynamically as a function of the position and orientation of the plane wavefronts. The velocity averaging is done using a Gaussian weight curve, centered at the wavepath location (see Figure 1). Equation (1) expresses the wavelength averaged velocity \bar{v} at a point (\vec{x}_v) for a wave

Figure 1: Waveray wavepath and wavelength-dependent velocity smoothing at point \vec{x}_v . Adapted from Lomax (1994). hector-lomax1
[NR]



period \mathbf{T} (Lomax, 1994),

$$\bar{v}(\vec{x}_v, \mathbf{T}) = \frac{\int_{-\infty}^{\infty} \omega(\gamma) c[\vec{x}(\gamma, \mathbf{T})] d\gamma}{\int_{-\infty}^{\infty} \omega(\gamma) d\gamma} \quad (1)$$

where γ is the arc length along the wavefront away from \vec{x}_v expressed in wavelengths. $c(\vec{x})$ is the velocity at point \vec{x} and $\omega(\gamma)$ is the Gaussian weight curve:

$$\omega(\gamma) = e^{-4\ln 2 \cdot (\gamma/\alpha)^2} \quad (2)$$

where α specifies the half width of the Gaussian bell in wavelengths. $(\vec{x}(\gamma, \mathbf{T}))$ is the position along the instantaneous straight wavefront given by the recursive relation (Lomax, 1994):

$$\vec{x}(\gamma, \mathbf{T}) = \vec{x}_v + \frac{\mathbf{T}}{2\pi} \int_0^\gamma c[\vec{x}(\gamma', \mathbf{T})] \hat{\mathbf{n}}(\mathbf{T}) d\gamma' \quad (3)$$

where $\hat{\mathbf{n}}$ is the unit normal to the wavepath at point \vec{x}_v . The discrete representation of equation (1) is given by equation (4):

$$\bar{v}(\vec{x}_v, \mathbf{T}) = \frac{\sum_{n=-N}^N \omega_n c[\vec{x}_v^n(\mathbf{T})]}{\sum_{n=-N}^N \omega_n} \quad (4)$$

where the integral has been replaced by a finite sum over $2N + 1$ **control points**. The position of the control points along the wavefronts are given by equations (5) and (6).

$$\vec{x}_v = \vec{x}_v^0 \quad (5)$$

$$\vec{\mathbf{x}}_v^n = \begin{cases} \vec{\mathbf{x}}_v^{n-1} + \frac{\gamma_{max}}{4\pi N} \lambda(\vec{\mathbf{x}}_v^{n-1}) \hat{\mathbf{n}} & n = 1, 2, \dots, N. \\ \vec{\mathbf{x}}_v^{n+1} - \frac{\gamma_{max}}{4\pi N} \lambda(\vec{\mathbf{x}}_v^{n+1}) \hat{\mathbf{n}} & n = -1, -2, \dots, -N. \end{cases} \quad (6)$$

These two equations are the discrete version of equation (3), but, the dependence on the wavelength has been made explicit. Notice that the subscript ν of $\vec{\mathbf{x}}_v^n$ runs along the wavepath and the superscript n runs along the wavefront. γ_{max} specifies the largest distance in wavelengths along the wavefront at which smoothing is applied. The discrete equivalent of the Gaussian weight function is:

$$\omega_n = e^{-4 \ln 2 \cdot (\gamma_n / \alpha)^2} \quad (7)$$

where the distance γ_n along the wavefront in wavelengths is expressed as:

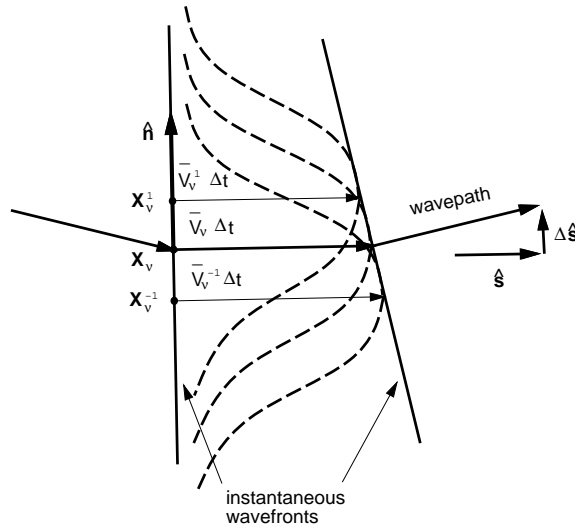
$$\gamma_n = \frac{n \gamma_{max}}{N} \quad (8)$$

The motion of the waverays along the direction of propagation is expressed by the following equation:

$$\vec{\mathbf{x}}_{v+1} = \vec{\mathbf{x}}_v + \bar{v}_v \Delta t \hat{\mathbf{s}} \quad (9)$$

where $\bar{v}_v = \bar{v}(\vec{\mathbf{x}}_v, \mathbf{T})$, Δt is the time step and $\hat{\mathbf{s}}$ is a unit vector that moves along the direction of propagation. The change in direction of the waverays is approximated by the difference in

Figure 2: Waveray wavepath calculation. Huygen's principle is used to obtain the bending $\Delta \hat{\mathbf{s}}$ of the wavepath from points $\vec{\mathbf{x}}_v^1$ and $\vec{\mathbf{x}}_v^{-1}$. Adapted from Lomax (1994). [hector-lomax2](#) [NR]



movement between the first control point on either side of the wave location $\vec{\mathbf{x}}_v$, as shown in Figure 2:

$$\Delta \hat{\mathbf{s}} = - \left(\frac{\bar{v}_v^1 - \bar{v}_v^{-1}}{|\vec{\mathbf{x}}_v^1 - \vec{\mathbf{x}}_v^{-1}|} \right) \Delta t \hat{\mathbf{n}} \quad (10)$$

where \bar{v}_v^1 and \bar{v}_v^{-1} are the wavelength averaged velocities at the wavefront points $\vec{\mathbf{x}}_v^1$ and $\vec{\mathbf{x}}_v^{-1}$ respectively. Finally, the half width parameter α and the truncation parameter γ_{max} are set at $\alpha = 2.0$ and $\gamma_{max} = 1.5$, based on Lomax's (1994) calibration. The number of control points N is set proportional to the ratio $T/\Delta t$ of the wave period over the time step. Figure 3 shows

the significant differences between the waveray and ray methods. Notice how a high frequency ray is scattered by the small velocity anomaly, while the waveray's wavepath is little deflected. Note also, how the third ray (from right to left) is not perturbed by the low velocity anomaly, while the waveray wavepath is deflected. The wavelength-dependent velocity averaging smoothes out small velocity variations and causes the wavepath to be affected from velocity variations away from it.

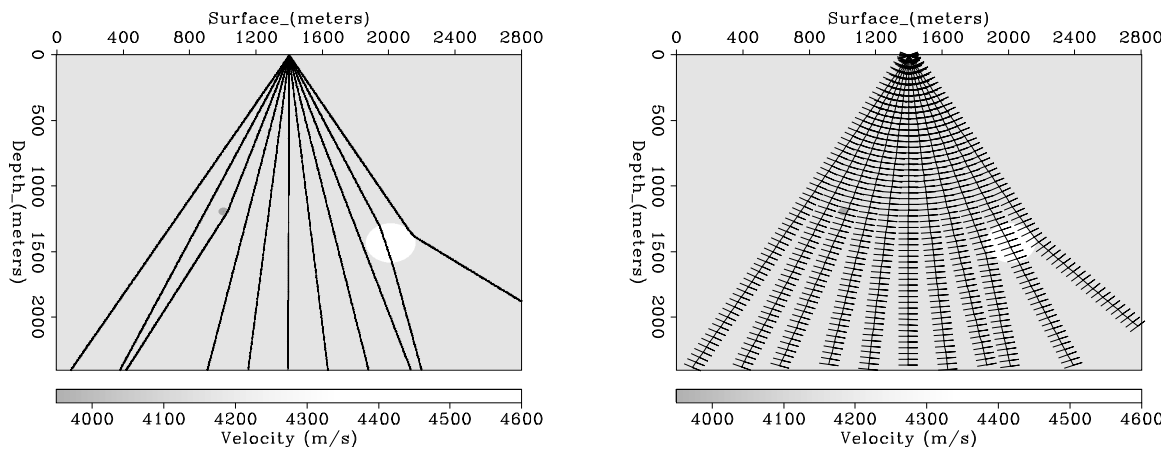


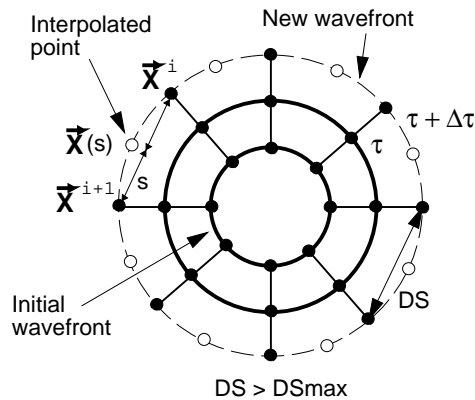
Figure 3: Left frame shows a fan of high frequency ray paths. Right frame shows a fan of 12 Hz waveray wavepaths. The straight segments perpendicular to the waverays represent the instantaneous wavefronts. The velocity model is defined by two circular anomalies drawn in a homogeneous background. The black dot (located at 1000 m. by 1250 m. in depth) depicts a low velocity anomaly. The white circle a high one. [hector-lomaxsbs](#) [NR]

NORSAR WAVEFRONT CONSTRUCTION

The main idea behind the “NORSAR” method (1993) is to compute ray parameters along wavefronts instead of computing them from independently traced rays, as conventional ray methods do. Wavefronts are defined as isochron traveltimes curves (lines in 2-D) from the source. New wavefronts are constructed from previous ones, by ray tracing over a time step. As wavefronts expand out, new rays are interpolated between rays that go further apart than a predefined distance DS_{max} . Figure 4 illustrates how wavefronts expand out, by ray tracing from a time τ to a time $\tau + \Delta\tau$. The dashed line on Figure 4 represents the new wavefront. The solid dots represent the end points of the rays. The distance between contiguous end points is checked against the predefined maximum distance DS_{max} . If they are located further than DS_{max} , a new point (empty dots) is interpolated. The interpolation of these new points over the wavefront is done using a vectorial third order polynomial $\vec{x}(s) = \vec{a}s^3 + \vec{b}s^2 + \vec{c}s + \vec{d}$. The polynomial is evaluated as a function of the normalized distance s between points \vec{x}^i and \vec{x}^{i+1} . Also a scalar third order polynomial is used to interpolate amplitude values and the ray’s angle of direction (see Vinje et. al. (1993)). The key property of this procedure is that it produces a fairly constant density of rays over C1 models (Vinje et al., 1993) (see Figure 8), illuminating zones with high geometrical spreading where conventional ray tracing have shadow zones. Rays are eliminated if they go out of the model boundaries. They may also be eliminated if a

Figure 4: New wavefronts (dashed lines) are constructed from the previous wavefront (solid line), by ray tracing a fix number of time steps. New rays are interpolated between points on the wavefront that lay further than a predefined distance. Adapted from Vinje et. al. (1993).

`hector-norsar1` [NR]



wavefront crosses over itself, as shown on Figure 5. The “self-crossing” of the wavefronts may correspond to a caustic or to the intersection of rays from different parts of the model. Once again, as in the Lomax algorithm, for the sake of computational time and also of memory, a “first arrival” mode should be used. This first arrival mode removes all later arrivals. When the number of points in a wavefront becomes less than a certain value (e.g. 4 points), the algorithm stops. Traveltimes and amplitudes are interpolated into a rectangular grid. Ray cells, defined as the area enclosed by a pair of contiguous rays and wavefronts, are checked for the presence of grid points (see Figure 6). Traveltimes at the receivers are estimated by computing the following quantities:

1. the distances d_1 and d_2 from the receiver perpendicular to the two rays.
2. the normalized distance s along the wavefront $s = d_1/(d_1 + d_2)$.

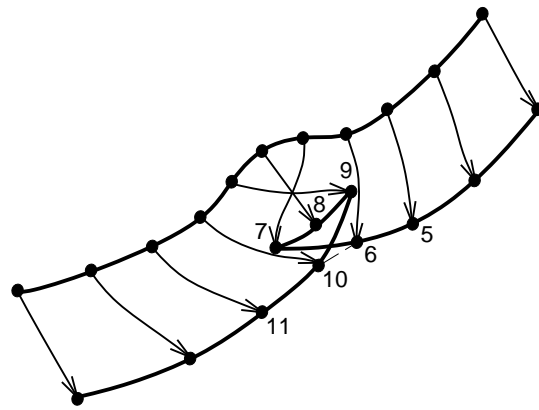
3. the interpolated point $\vec{x}(s)$ over the old wavefront.
4. the distance l_r from $\vec{x}(s)$ to the receiver
5. the velocity v_{mid} in the midpoint of the segment l_r .

The traveltimes at the receiver is then estimated to be:

$$t_{rec} = t + \frac{l_r}{v_{mid}} \quad (11)$$

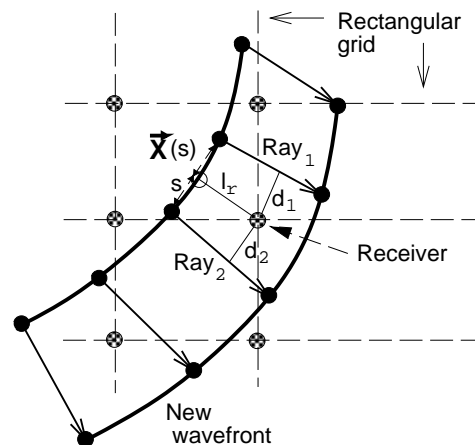
where t is the traveltimes to the old wavefront. In computing amplitudes, the geometrical

Figure 5: The new wavefront crosses itself. If only first arrivals are wanted, the points behind the crossing (points no. 7, 8, 9) are removed from the wavefront. Adapted from Vinje et. al. (1993). [hector-norsar2](#) [NR]



spreading factor $\sqrt{(r_1 + r_2)/(R_1 + R_2)}$, gives the ratio between the amplitude of one wavefront to the next one. R_1 , R_2 , r_1 and r_2 are shown on Figure 7. The amplitude estimation at the receivers is also obtained in this way, where the distances d_1 and d_2 are used for R_1 and R_2 . Figure 8 shows an example of the Norsar method run over a highly contrasted velocity model. The velocity model is a pair of Gaussian bell curves. The distance between the peaks is 48 meters with a drop of 4 km/s in velocity. A final point on Norsar's method is, as said by Vinje

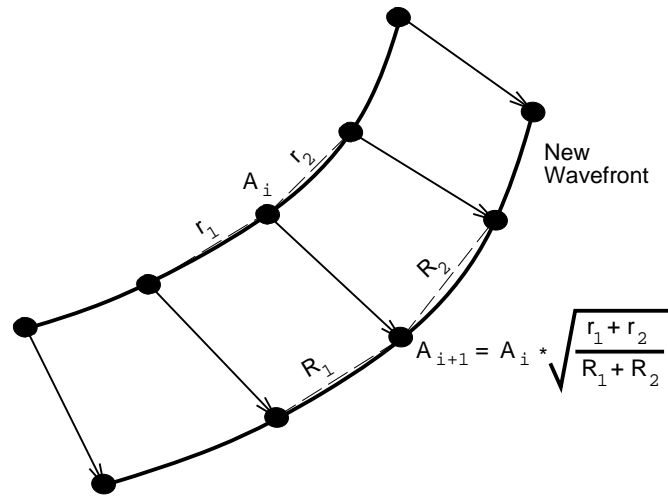
Figure 6: Traveltimes and amplitudes are found at receivers by interpolating within each ray cell. The ray cell is defined by Ray_1 and Ray_2 , and by the new wavefront and the previous wavefront. Adapted from Vinje et. al. (1993). [hector-norsar3](#) [NR]



et. al. (1993): “the way the ray tracing between each wavefront is performed is irrelevant to the idea of the wavefront construction”. We notice that all along the discussion on the NORSAR

method, ray tracing was kept as an abstract idea. With this in mind we proceed to merge the Lomax algorithm, as the ray tracing algorithm for the NORSAR method. Another advantage of the NORSAR method is that the estimation of ray parameters (as traveltimes, amplitudes, etc.) does not come from a posteriori interpolation between single, separate rays, but instead directly from previously constructed wavefronts.

Figure 7: Amplitudes are computed from the previous wavefront. The geometrical spreading factor gives the ratio between the amplitude A_i at the previous wavefront and the new amplitude value A_{i+1} . `hector-norsar4`
[NR]



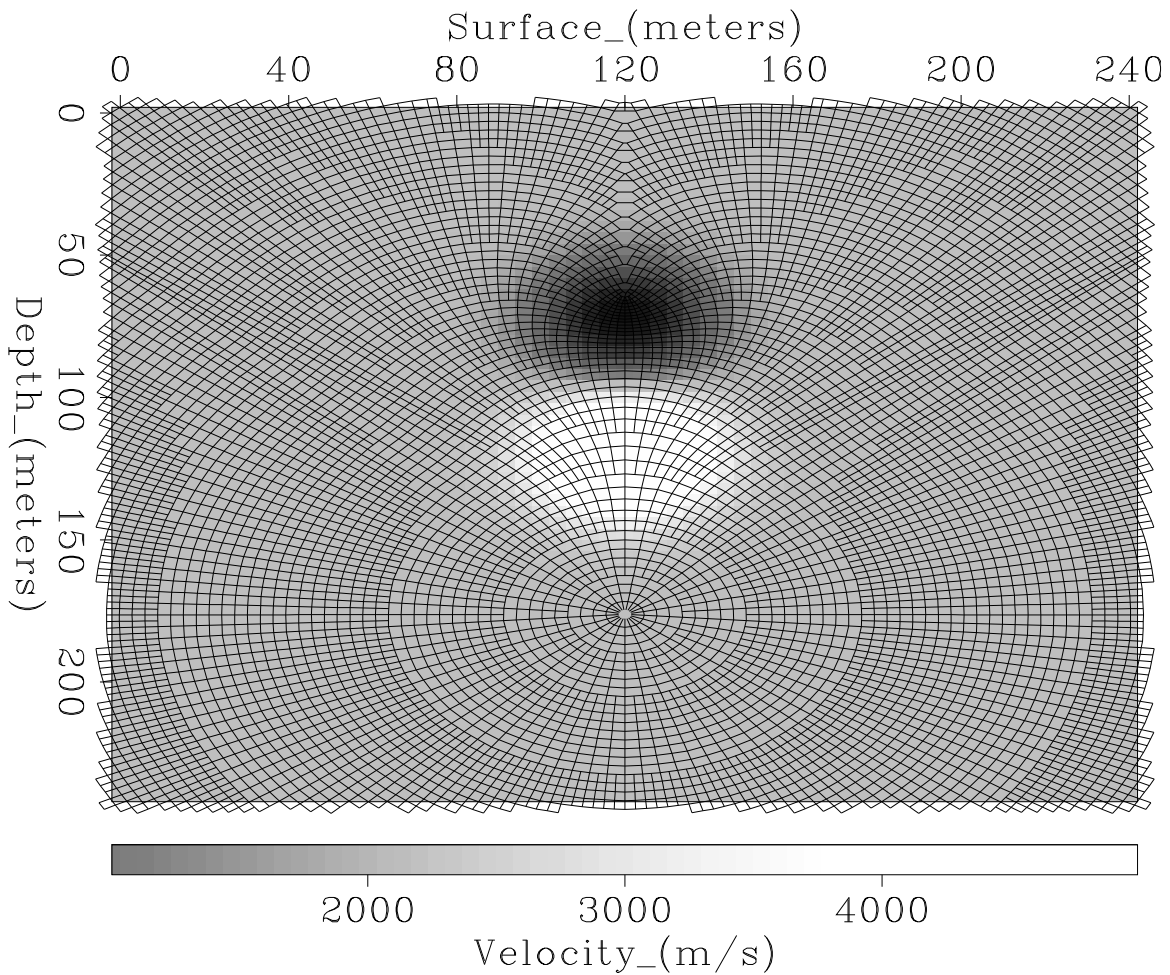


Figure 8: The “NORSAR” or wavefront construction method covers the whole model with wavefronts and rays. The model presents a strong variation in velocity, given by a Gaussian bell with a maximum amplitude of 5000 m/s and a second Gaussian bell with a minimum amplitude of 1000 m/s. The background is 3000 m/s. `hector-gauss-wv` [ER,M]

WAVERAYS AND WAVEFRONTS

The product of merging the two previously discussed ray tracing methods is sketched in the following pseudo-code:

```

1  Allocate memory for wavefronts and output
2  for each source
3      initialize
4      while number of points in wavefront > 4
5          propagate wavefront
6          check for self crossing
7          check for rays that go out of bounds
8          eliminate self crossing and outofbound rays
9          calculate amplitudes
10         gridding
11         interpolate new rays
12         movwavf

```

The algorithm defines the data structure “*cube*” at line 1. In it, the ray parameters are stored as wavefronts propagate.

```

struct heptagon {
    struct point {
        float x;
        float z; } x0, x1;
    float angle;
    float ampl;
    char cf; } *cube;

```

where:

- *cube*[ii].x0 contains the starting position of a ray on a wavefront at a time τ .
- *cube*[ii].x1 contains the arriving position of a ray on a wavefront at a time step later, $\tau + \Delta\tau$.
- *cube*[ii].angle gives the arriving angle at point *cube*[ii].x1.
- *cube*[ii].ampl is the computed amplitude at point *cube*[ii].x1.
- *cube*[ii].cf is a flag that defines if point *cube*[ii].x1 is in bounds, out of bounds, or belongs to the inner section of a self crossing wavefront.

The index ii runs over the points of a wavefront. Since there is no a priori way of determining how large can a wavefront grow over a velocity model, a predefined limit (*nrmax*) of *cube*

elements is established at the beginning of the algorithm, which defines the total memory allocated for *cube*. In other words, *nrmax* is the maximum number of points that a wavefront can have. If the wavefront grows bigger than *nrmax* points the algorithm is stopped and an error message is produced indicating that a bigger value for *nrmax* should be used. This integer depends directly on the maximum allowed separation *DSmax* between two contiguous points in the wavefront. For the examples shown on Figure 9 through 12, the program ran with a value of *nrmax*=1300. *DSmax* was set to 21 meters for those examples. In the case that the algorithm is run in a “all arrivals” mode, which could be done by eliminating line 6 out of the algorithm, the number of crossing points on a wavefront could become considerably large. As the wavefronts cross and cross many times over itself, for a velocity model with strong variations (as for example the Marmousi model), the number of crossing points can easily reach the 6 digits figure. This translates directly into a bigger need of computer resources, in use of memory and time. Subroutine *initialize* defines the initial wavefront. It assigns an initial amplitude and take-off angle to the points on the initial wavefront. The *propagate wavefront* subroutine ray traces using Lomax’s waverays. The waverays are traced starting at *cube*[ii].x0 with a take-off angle *cube*[ii].angle during one time step at a certain frequency. The time step and the frequency are user predefined. Subroutine on line 6 checks for self crossed wavefronts and flags the points that belong to the inner crossed section of the wavefront. Line 7 checks for points that fall out of boundaries, raising a flag. Notice from Figure 8 that the rays cross over the boundaries of the model. This is done in order to obtain arrivals at the receivers that lie on the boundaries. Subroutine at line 8 eliminates the points on a wavefront that are flagged for laying out of bounds or belong to self crossed wavefronts. Subroutines on lines 9, 10 and 11 are implemented as previously explained for the NORSAR method on Figures 7, 6 and 4 respectively. On line 11 the number of rays that may be interpolated between any two contiguous rays, is given by the number of times the distance between the two rays is bigger than the maximum allowed distance *DSmax*. Subroutine *gridding* is a very time consuming, due to the irregular distribution of the data in the model. First, the subroutine checks for receivers inside the ray cells of two contiguous wavefronts. If a receiver is found, the ray parameters are interpolated to it. Subroutine *movwavf* prepares the structure *cube* for a new wavefront to be propagated. It takes as the new starting point the previous arriving point (*cube*[ii].x0 = *cube*[ii].x1).

Travel-times and amplitudes in the Marmousi model

Figures 9 to 12 display the results of a simulation that used the combined method. The underlying subsurface structure is the Marmousi model (Versteeg, 1993). A source was put at the surface, 5200 meters away from the left edge of the model, and the wavefronts were propagated until they crossed the boundaries of the model. Figure 9 shows the first-arrival traveltimes contours calculated at a frequency of 80 Hz. Figure 10 shows the same experiment at a frequency of 10 Hz. Not much difference is apparent. Figure 11 shows the amplitude estimates for the 80 Hz shot and Figure 12 shows the 10 Hz estimates. We see that more energy gets propagated down in the case of the low frequency, illuminating part of the high frequency shadow zones. We have seen that the combined method accomplishes two important tasks, it can be used to compute first arrival traveltimes and amplitudes over any general velocity

model and is it able to illuminate high frequency shadow zones. For these experiments, the mesh of the model is re-sampled from the original model at 8 x 8 meters. The traveltimes and amplitude outputs are placed in a mesh of 25 x 12.5 meters.

CONCLUSIONS

I have presented a review of two ray tracing methods. I have implemented both of them in a combined version. The method computes first arrival travel-times and amplitudes of seismic waves in complex 2-D velocity structures. The method uses a wavefront construction technique that produces a complete coverage of the medium by a fairly constant density of wavefronts and rays. Wavefronts are propagated using a wavelength-dependent smoothing ray tracing technique, called the waveray method, which leads to an increased stability of the ray paths relative to high frequency rays. Also, it gives a sensitivity to the rays to larger velocity anomalies that lay within a fraction of a wavelength of the ray path. The data (traveltimes and amplitudes) is computed on an irregular grid. As the wavefronts are constructed the data is interpolated into a regular grid. The result is a very robust ray tracing method that is able to illuminate areas of large geometrical spreading zones where conventional ray tracing methods produce shadow zones. Portions of the diffracted energy is produced in these shadow zones. Further work should be done on calibrating and testing the results produced by the combined method against other methods. Future work should be done on a formal derivation of the waveray method. Production of seismograms and a 3-D version are also sources of future work.

REFERENCES

- Červený, V., 1987, Ray tracing algorithms in three-dimensional laterally varying layered structures: D. Reidel Publ. Co.
- Dines, K. A., and Lytle, R. J., 1979, Computerized geophysical tomography: *Proc. IEEE*, **67**, no. 7, 1065–1073.
- Julian, B. R., and Gubbins, D., 1977, Three-dimensional seismic ray tracing: *J. Geophys.*, **43**, 95–114.
- Lomax, A., 1994, The wavelength-smoothing method for approximating broad-band wave propagation through complicated velocity structures: *Geophys. J. Int.*, **117**, no. 2, 313–334.
- Moser, T. J., 1991, Shortest path calculation of seismic rays: *Geophysics*, **56**, no. 1, 59–67.
- Podvin, P., and Lecomte, I., 1991, Finite-difference computation of traveltimes in very contrasted velocity model: A massively parallel approach and its associated tools: *Geophys. J. Int.*, **105**, 271–284.
- van Trier, J., and Symes, W. W., 1991, Upwind finite-difference calculation of traveltimes: *Geophysics*, **56**, no. 6, 812–821.
- Versteeg, R. J., 1993, Sensitivity of prestack depth migration to the velocity model: *Geophysics*, **58**, no. 6, 873–882.
- Vidale, J. E., 1990, Finite-difference calculation of traveltimes in three dimensions: *Geophysics*, **55**, no. 5, 521–526.
- Vinje, V., Iverson, E., and Gjøystdal, H., 1993, Traveltime and amplitude estimation using wavefront construction: *Geophysics*, **58**, no. 8, 1157–1166.

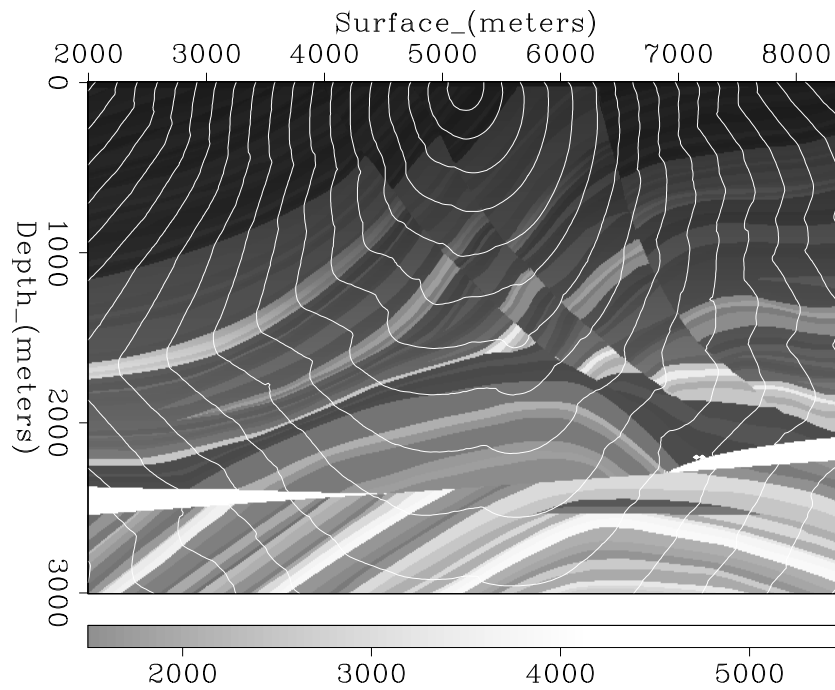


Figure 9: Traveltime contours computed from the combined method, overlaid on a section of the Marmousi model. A frequency of 80 Hz is used. `hector-marm80-time` [ER,M]

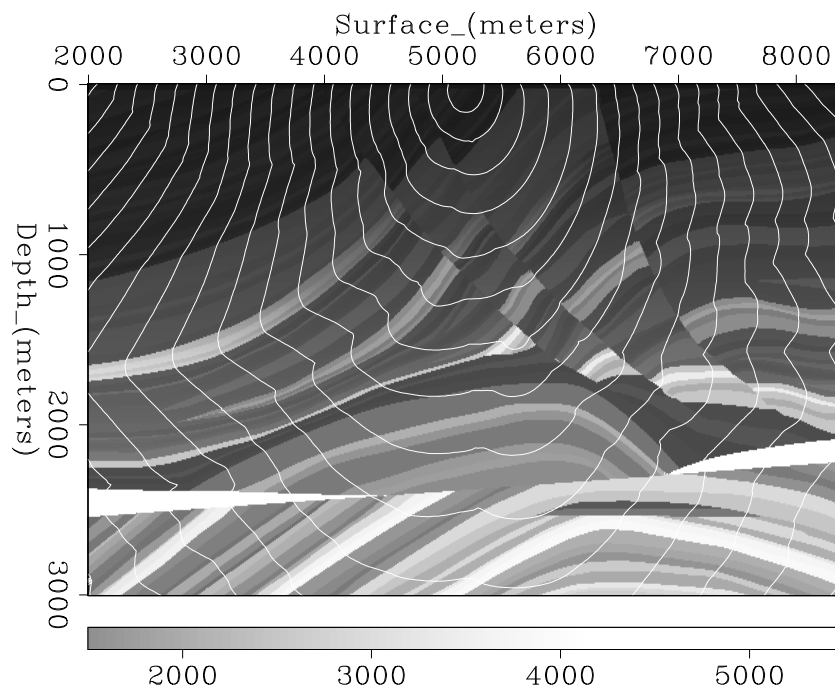


Figure 10: As in the previous Figure, but for a frequency of 10 Hz. `hector-marm10-time` [ER,M]

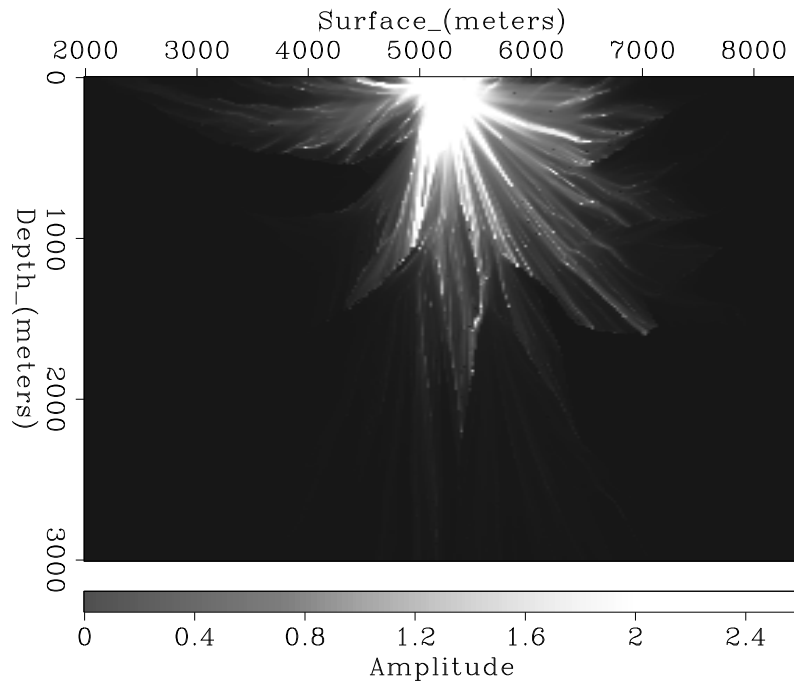


Figure 11: Amplitude maps from the combined method at a frequency of 80 Hz. `hector-marm80-ampl` [ER]

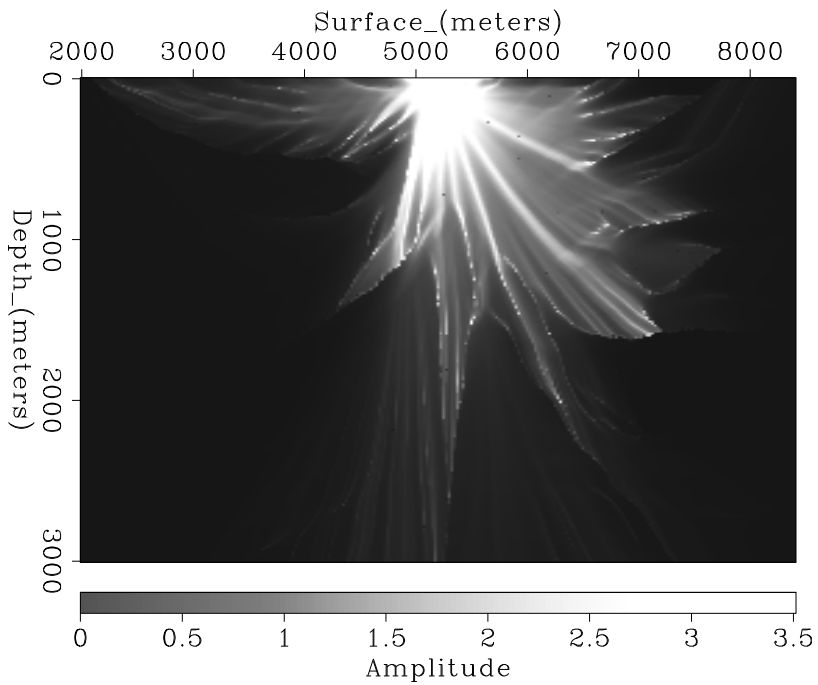


Figure 12: As in the previous Figure, but for a frequency of 10 Hz. `hector-marm10-ampl` [ER]